The effect of polyol on multiple ligand capped silver alloyed nanobimetallic particles in tri-*n*-octylphosphine oxide and oleic acid matrices

2016 Adv. Nat. Sci: Nanosci. Nanotechnol. 7 045012

(http://iopscience.iop.org/2043-6262/7/4/045012)

OPEN ACCESS
IOP Publishing | Vietnam Academy of Science and Technology
Advances in Natural Sciences: Nanoscience and Nanotechnology
Adv. Nat. Sci.: Nanosci. Nanotechnol. 7 (2016) 045012 (11pp)
doi:10.1088/2043-6262/7/4/045012

The effect of polyol on multiple ligand capped silver alloyed nanobimetallic particles in tri-*n*-octylphosphine oxide and oleic acid matrices

Joseph Adeyemi Adekoya[1,2], Enock Olugbenga Dare[3], Kehinde Olurotimi Ogunniran[1], Tolutope Oluwasegun Siyanbola[1], Olayinka Oyewale Ajani[1], Cyril Osereme Ehi-Eromosele[1] and Neerish Revaprasadu[2]

[1] Department of Chemistry, Covenant University, P. M. B. 1023, Ota, Ogun State, Nigeria
[2] Department of Chemistry, University of Zululand, Private Bag X1001, Kwa-Dlangezwa 3886, South Africa
[3] Department of Chemistry, Federal University of Agriculture, Abeokuta, Nigeria

E-mail: joseph.adekoya@covenantuniversity.edu.ng

Received 4 July 2016
Accepted for publication 4 August 2016
Published 13 October 2016

Abstract

The syntheses of Ag/M (M is Co, Ni, Pd, Pt and Ru) alloyed nanobimetallic particles in tri-*n*-octylphosphine oxide and oleic acid matrices were successfully carried out by the successive reduction of ligand capped metal ions with polyols, which resulted in rapid precipitation of some fractal high index faceted hybrid Ag/M bimetal nanoparticles. The optical measurements revealed the existence of modified surface plasmon band and peak broadening resulting from reaction-limited growth processes of the metal sols, making it possible to monitor the changes spectrometrically. The bimetallic nanoparticles were further characterized by powder x-ray diffraction, x-ray photoelectron spectroscopy and electron microscopy techniques which confirmed the formation of novel core–shell and alloyed clusters. The Ag/M nanoparticles thus synthesized within TOPO/OA matrices indicated significant reduction potential as a result of their energy band gap 2.65–2.77 eV which points to the fact that they could serve as reducing agents for electrocatalytic reaction.

Keywords: tri-*n*-octylphosphine oxide, oleic acid, matrices, alloyed silver nanobimetallic particles, capping agent, electron micrographs
Classification numbers: 2.00, 2.03, 4.00, 4.02, 5.03

1. Introduction

The synthesis and characterization of novel functional nanomaterials has dominated the field of materials science during the past decade. Initial work on isolated nanoparticles is now being superseded by the assembly of nanoparticles into 1D, 2D and 3D structures. The ultimate goal of this approach is to explore the collective physical properties of the assemblies, which are different from those of isolated materials. To this end, various strategies such as solvent evaporation, electrostatic attraction, hydrogen bonding, DNA-driven assembly, and cross-linking induced by bio-specific interaction like antigen–antibody have been developed to form nanoparticle assemblies and to harness their properties in the fabrication of nanostructured devices [1].

The structural or electronic property of binary nanoparticles is different from that of their individual parent

components thereby enhancing their activity or stability [2, 3]. They are particularly important in the field of catalysis since they often exhibit better catalytic properties than their monometallic counterparts [4]. Amongst the various bimetallic materials, the Pd–Ag system is unique and interesting as it shows high activity towards useful chemical reactions e.g., hydrogenation of 4-pentenotic acid, acetoxylation of ethylene to vinyl acetate [5].

Although efforts have been made to study the synthesis of Ag/M bimetallic nanoparticles, the preparation of alloy structured Ag/M nanoparticles is still a challenge [6]. The synthesis of core–shell structured Ag/M nanostructures has been achieved using either sequential or the co-reduction method [7, 8].

Silver has been used in conjunction with metals such as palladium [9, 10] and platinum [11–13] for various catalytic reactions. The structure of bimetallic combinations depends mainly on the preparation conditions and the miscibility of the two components. Combinations such as Ag/Pd and Ag/Pt have been reported to exhibit a core–shell structure while Au/Ag forms either a core–shell [14, 15] or an alloy phase [16, 17] depending on the preparation conditions. Ksar *et al* [18] have reported a radiolytic reduction method, by which, Pd/Au alloy nanoparticles stabilized by poly(acrylic acid) were prepared. Mejía-Rosales *et al* [19] synthesized and characterized Pd/Au nanoparticles passivated by poly(vinlpyrrolidone) (PVP) using a sequential reduction protocol. When hydrazine was used as a strong reductant, PVP protected Pd/Au alloy nanodendrites with an average particle size of 15–26 nm have been synthesized. Similarly, Suo and Hsing [20] reported a simple co-reduction method, in which ethylene glycol and sodium citrate were utilized as the reducing and stabilizing agents respectively to synthesize Pd/Au bimetallic nanoparticles.

The utilization of a wide variety of protective reagents such as polymers [21], mercaptans [22–26] and microemulsions [27] to prevent the nanoparticles produced in the liquid phase from aggregation is an advantage of the ligand mediated synthesis route. More recently, Adekoya *et al* [28] prepared novel silver alloyed nanoparticles via polyol reduction in hexadecylamine (HDA) capping ligand matrix. Ag/Pd and Ag/Pt nanoparticles of novel alloy morphology with average diameters of 20.60 ± 0.97 and 10.36 ± 1.73 nm, respectively, were achieved. However, the need to control key morphological properties of the nanoparticles has made it imperative to introduce the concept of multiple ligand capping.

In this work we report a simple co-reduction method with ethylene glycol or glycerol as the reducing agent and tri-*n*-octylphosphine oxide/oleic acid as combined stabilizing agent to synthesize M (Co, Ni, Pd, Pt, Ru)/Ag bimetallic nanoparticles. Traditionally, the formation of M/Ag core–shell/alloys through concurrent reduction of M and Ag ions is not easy because of the vast difference of redox potentials between the two species considered. At the same reducing environment, Ag ions have much higher reduction rate than that of M (Co, Ni, Pd, Pt, Ru) ions. To overcome this limitation, our approach was to adopt and extend the principle of

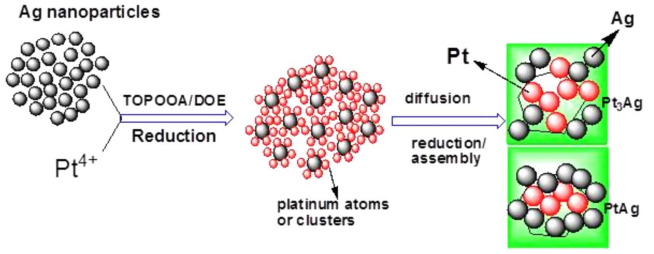

Scheme 1. Seed growth mechanism for synthesizing high faceted silver allied bimetallic nanoparticles.

reaction engineering and rate-limiting strategy enunciated by Suo and Hsing [20] to carefully control the synthesis environment that would enable the production of alloy and core–shell M/Ag bimetallic nanoparticles. M/Ag alloy nanoparticles with different metallic compositions were successfully synthesized by this new approach (scheme 1).

The multiple ligands tri-*n*-octylphosphine oxide and oleic acid matrices as organic capping ligands act as templates for the moderate temperature reduction of metal salt precursors mediated by polyol through the initial heterogeneous nucleation and rapid particle growth processes to form self-assembled silver alloyed hybrid nanoparticles with tuneable morphology. By choosing concentrations of these particles, their size distribution, the conditions of solvent evaporation, its ionic strength and the organic chelating ligand concentration, one, two or three-dimensional structures can be obtained [29]. The long chain aliphatic end of oleic acid and the oxygen of the phosphine ligand are the template and binding site respectively for the formation of an adduct molecule or seed which is consequently reduced or hydrolysed to the metal zero-valent state. The seed growth mechanism is therefore proposed to give the desired bimetallic nanoparticles through successive nucleation and condensation processes (see scheme 1).

2. Experimental

The co-precipitation or successive reduction method involving seed growth and subsequent rapid diffusion of nucleated seeds deployed in this work was modified from previous work [30] and used to prepare monodispersed Ag/M alloyed nanoparticles at optimum concentration of metal precursors under controlled temperature conditions. The reactions for the reduction of metal ion in liquid phase are as follows [31]:

$$Pt + CH_3OH \rightarrow Pt - (COH)_{ads} + 3H^+ + 3e^-,$$

$$Pt - (COH)_{ads} + H_2O \rightarrow Pt + CO_2 + 3H^+ + 3e^-,$$

$$[PtCl_4]_{(aq)} + 4Ag_{(s)} \rightarrow Pt_{(s)} + 4Ag^+_{(aq)} + 4Cl^-_{(aq)},$$

$$Ag^+_{(aq)} + Pt_{(s)} \rightarrow Ag_{(t)}Pt_{(s)}.$$

The reaction mechanism for the formation of bimetallic nanoparticles via the anisotropic heterogeneous nucleation and growth mechanism is shown in scheme 2.

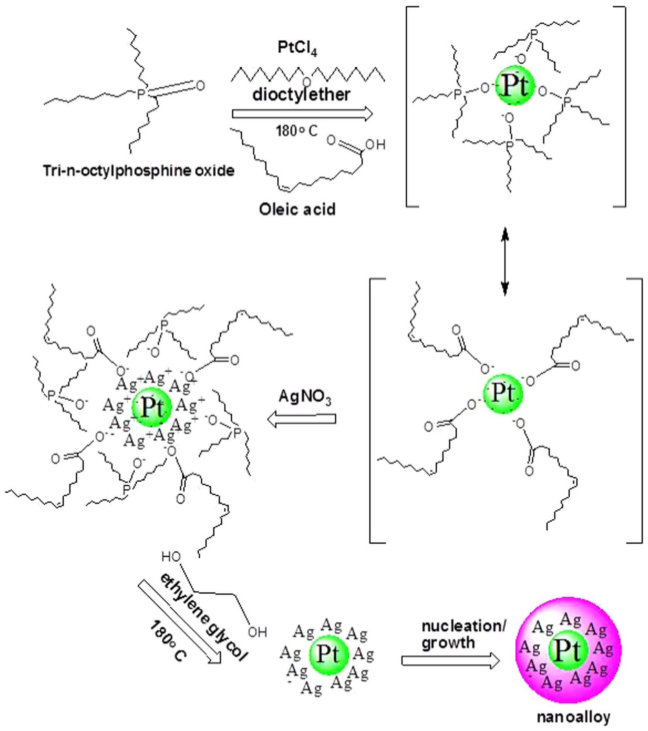

Scheme 2. Anisotropic reduction and nucleation processes of Ag/M allied nanohybrid leading to alloy structure.

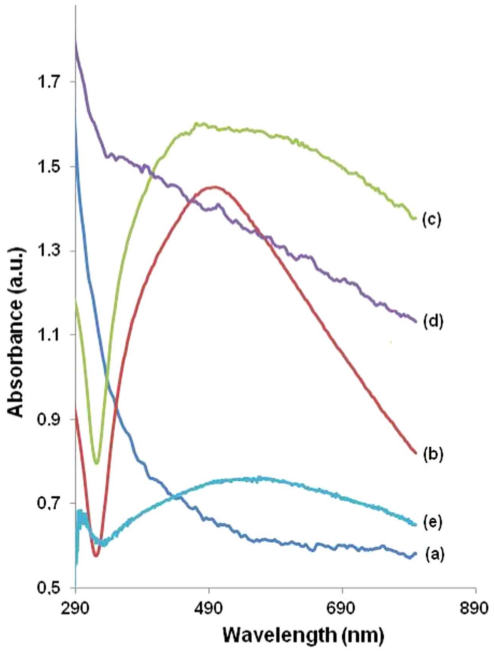

Figure 1. UV–vis spectra of Ag allied bimetallic sols capped with TOPO/OA at 180 °C, 2 h: (a) AgPd-TOPO/OA, (b) AgNi-TOPO/OA, (c) AgCo-TOPO/OA, (d) AgPt-TOPO/OA and (e) AgRu-TOPO/OA.

2.1. Materials

All inorganic salts, solvents and chemical reagents used were analytical grade, and were purchased from Sigma-Aldrich Corporation, UK. They are as follow: tri-*n*-octylphosphine oxide (TOPO), oleic acid (OA), silver nitrate, nickel(II) acetate, cobalt(II) acetate, palladium(II) chloride, platinum (IV) chloride, ruthenium(III) chloride, dioctylether (DOE), glycerol (GLY), ethylene glycol (EG), methanol (99.5%.w/w) and (99.5%.w/w) ethanol.

2.2. Synthesis of alloyed Ag/M nanoparticles

Fractal monodispersed bimetallic Ag/M (M = Co, Ni, Ru, Pd, Pt) nanostructured particles were prepared by the seed growth or successive addition method [15, 32]. Briefly, 6.162–6.278 g (15.94–16.25 mmol), 99%w/w TOPO (capping agent) was measured into a round bottom flask containing a magnetic stirrer and it was gradually heated to melt. 4.475 g (15.75 mmol) oleic acid (OA) was added as dispersing solvent. The mixture was stirred and gradually heated at the rate of 2.0 °C min^{-1} to 200 °C followed by the injection of 0.140 g (0.56 mmol) $Co(CO_2CH_3)_2.4H_2O$ dispersed in 5.0 ml dioctylether and 5.0 ml ethylene glycol (EG) or glycerol (GLY) as reducing agent. A rapid colour change to brown was observed. The resultant mixture was left to allow for the growth of Co nanoparticles which also acted as a seed for the next reaction. Then, 0.069–0.144 g (0.41–0.85 mmol) $AgNO_3$ similarly dispersed in 5.0 ml dioctylether (DOE) was injected into the colloidal mixture, followed by hot injection of 5.0 ml aliquot of ethylene glycol. The reaction continued for 2 h with continuous stirring. After the hot injection of silver nitrate solution, a shiny brown coloured Ag/Co sol was obtained. While hot, the Ag/Co sol was copiously washed with methanol several times, and centrifuged at 4400 rpm for 10–15 min to remove excess unreacted stabilizer. The Ag/Co sol was later redispersed in ethanol.

The procedure was subsequently repeated for other molecular precursors: 0.165 g (0.66 mmol) $Ni(CO_2CH_3)_2.4H_2O$; 0.048 g (0.23 mmol) $RuCl_3$; 0.071 g (0.40 mmol) $PdCl_2$; 0.074 g (0.22 mmol) $PtCl_4$ to produce Ag/Ni, Ag/Ru, Ag/Pd and Ag/Pt TOPO/OA capped nanocomposites respectively. The centrifuged sol obtained after decantation was redispersed in ethanol and cleaned in ultrasonic bath at 50 °C for 60 min before further characterization.

2.3. Characterization

Optical characterization was done using a UV–vis spectrophotometer (Varian Cary 50 Conc) to carry out the optical measurements and the samples were placed in silica cuvettes (1 cm path length), using toluene as a reference solvent. A luminescence spectrometer (Perkin-Elmer LS 55) was used to measure the photoluminescence of the particles. The samples were placed in a quartz cuvette (1 cm path length).

The crystalline phase was identified by x-ray diffraction (XRD), employing a scanning rate of 0.05° min^{-1} in a 2θ range from 20° to 80°, using a diffractometer (Bruker AXS D8) equipped with nickel filtered Cu-$K\alpha$ radiation (λ = 1.5406 Å) at 40 kV, 40 mA and at room temperature. The morphology and particle sizes of the samples were characterized by a JEOL 1010 TEM with an accelerating voltage of 100 kV, Megaview III camera, and Soft Imaging

Table 1. Comparison of the properties of synthesized silver alloyed nanobimetallic particles in tri-*n*-octylphosphine oxide and oleic acid matrices.

Ag/M nanoparticle	Temperature of reaction (°C)	Amount precursor M_1/M_2/stabilizer (mmol)	Time reaction (min)	Size nanoparticle (nm)	Absorbance λ_{max}/bandgap (nm eV^{-1})
Ag/Co/TOPO/OA	200	1:1:32	120	7.02 ± 1.64	447/2.77
Ag/Ni/TOPO/OA	200	1:2:39	120	22.21 ± 10.27	462/2.68
Ag/Ru/TOPO/OA	200	2:1:71	120	23.07[a]	467/2.66
Ag/Pd/TOPO/OA	200	2:1:41	120	16.50 ± 9.72	465/2.67
Ag/Pt/TOPO/OA	200	4:1:74	120	4.70 ± 0.93	469/2.65

[a] Size determination by p-XRD.

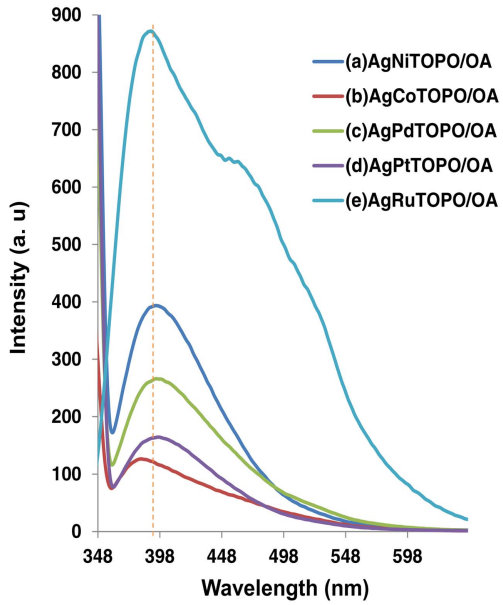

Figure 2. PL emission spectra of (a) Ag/Ni, (b) Ag/Co, (c) Ag/Pd, (d) Ag/Pt and (e) Ag/Ru TOPO/OA capped sols at 180 °C, 2 h; excited at 340 nm, each exhibiting emission peak between 378 and 387 nm.

Systems iTEM software. The detail morphological and structural features were investigated using HRTEM images with a JEOL 2010 TEM operated at an accelerating voltage of 200 kV. A cursory survey of surface property and high resolution spectra of nanoparticles were collected using XPS PHI 5000 Versaprobe-Scanning ESCA Microprobe, with 100 μm, 25 W, 15 kV Al monochromatic x-ray beams.

3. Results and discussion

The ligand capped nanoparticles were found to be very stable both in the liquid and solid phases. The stability was investigated by following the absorbance spectra over extended periods of 6 months, and reproducible absorption maxima were obtained typical of Ag/M sol property.

3.1. Optical properties of Ag/M sols

The UV–vis absorption spectra of Ag alloyed nanoparticles capped by TOPO/OA with different metal precursors/ligand mole ratios are shown in figure 1. The optimum stoichiometric ratios for the co-precipitation reactions which produced the TOPO/OA capped Ag alloyed bimetallic sols with different metal precursors/capping agent mixtures are shown in table 1. At the approximate ratios, colloidal dispersions were formed which were easily re-dispersed in ethanol and the optical absorption of Ag alloyed metal sols was conveniently measured.

Furthermore, a trend was observed in TOPO/OA stabilized Ag alloyed bimetallic sols (figure 1). The surface plasmon band (SPB) for AgCo, AgNi and AgRu occurred at 447, 462 and 467 nm respectively, while it was almost extinct in the spectra of AgPd and AgPt sols, showing very weak band at 465 and 427 nm, respectively. Moreover, the SPB appeared broad with consequent shift towards the visible region. This was observed as result of contribution from multiple organic capping ligands made up of tri-*n*-octylphosphine oxide and oleic acid [24]. The phosphinate oxygen has a weaker binding effect, therefore, it is displaced by the carboxyl group of oleic acid [32, 33], thereby, accounting for the observed strong band and red electronic shift in the absorbance spectra of the TOPO/OA capped Ag alloyed bimetallic sols.

The absorption band gaps of the Ag/M sols which were estimated by the direct band gap method [34, 35], using the cut-off band edges from figure 1 are presented in table 1.

The absorption edges were red-shifted from that of Ag, Co, Ni, Ru, Pd and Pt bulk crystals given as 3.99 eV [36], 3.17 eV [37, 38], 5.20 eV [39], 3.2 eV [40], 7.6 eV [41] and 3.0 eV [42, 43].

The photoluminescence measurements of TOPO/OA capped Ag alloyed bimetallic sols was carried out in ethanol, the resulting emission spectrum (figure 2) was analysed to deduce relative position of emission spectra of the different Ag alloyed bimetallic sols. Generally, all the TOPO/OA capped bimetallic sols exhibited strong emission peak between 378 and 385 nm, strongly indicating occurrence of alloy formation with likelihood of surface enrichment by silver (Ag) atoms. Further excitation of the bimetallic sols at 232 and 325 nm showed no significant shift in the emission properties confirming the quantum properties of the as prepared nanosols according to Kasha rule [44] that the emission spectra of potential fluorophores are typically independent of excitation wavelength.

In TOPO/OA capped Ag/Ru sols (figure 2), the most intense emission peak was observed at 385 nm for an excitation at 340 nm which occurred at a little relatively lower wavelength than TOPO/OA capped Ag/Co sol, the difference observed can be attributed to the nature of electronic interaction between the metal core and chromophoric group in oleic acid and tertiary alkylphosphine used as capping agents [44, 45]. This effect usually results in fluorescent quenching [46], a phenomenon that leads to decrease in intensity is given by

$$F_0/F = 1 + K[Q] = 1 + K_q\tau_0[Q],$$

where F_0/F is decrease in fluorescence intensity, K is the Stern–Volner quenching constant, K_q is the bimolecular quenching constant; τ_0 is the unquenched lifetime, $[Q]$ is the quencher concentration.

It is apparent that fluorescent lifetime and quantum yield efficiency in Ag/Ru TOPO/OA capped sols can be used as a measure of their activity as sensors or actuators paving way for these new materials in effluent gas sensing.

3.2. Morphology of the Ag/M sols

The TEM image (figure 3(a)) and particle size distribution histogram (figure 4(a)) of TOPO/OA capped Ag/Co alloyed nanobimetallic particle reveal particles in the form of clusters monodispersed with a predominantly cubic or close to

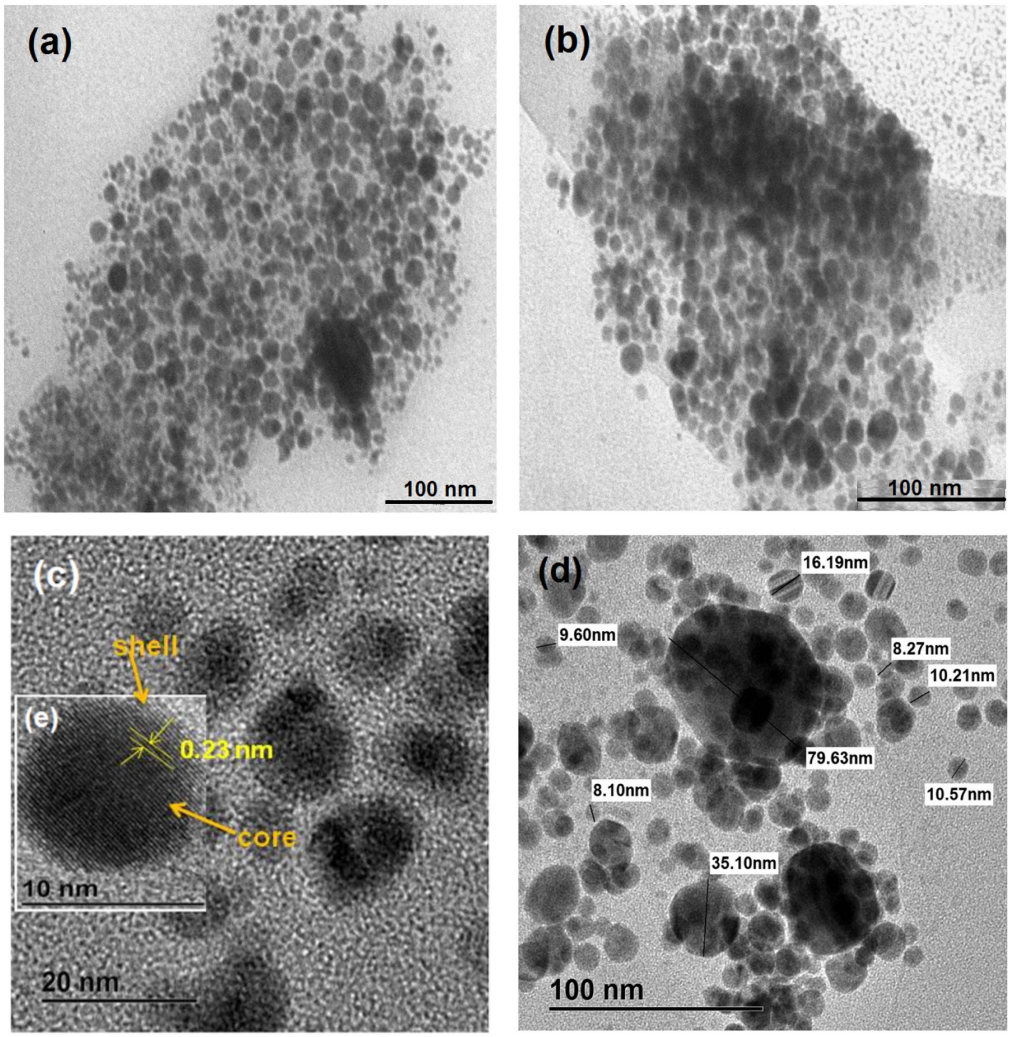

Figure 3. TEM images (a) Ag/Co NPs, (b) Ag/Ni NPs, (c), (d) HRTEM images of (a) and (b), respectively; inset (e) core–shell nanostructure of Ag/Co nanoparticles capped by TOPO/OA at 180 °C, 2 h.

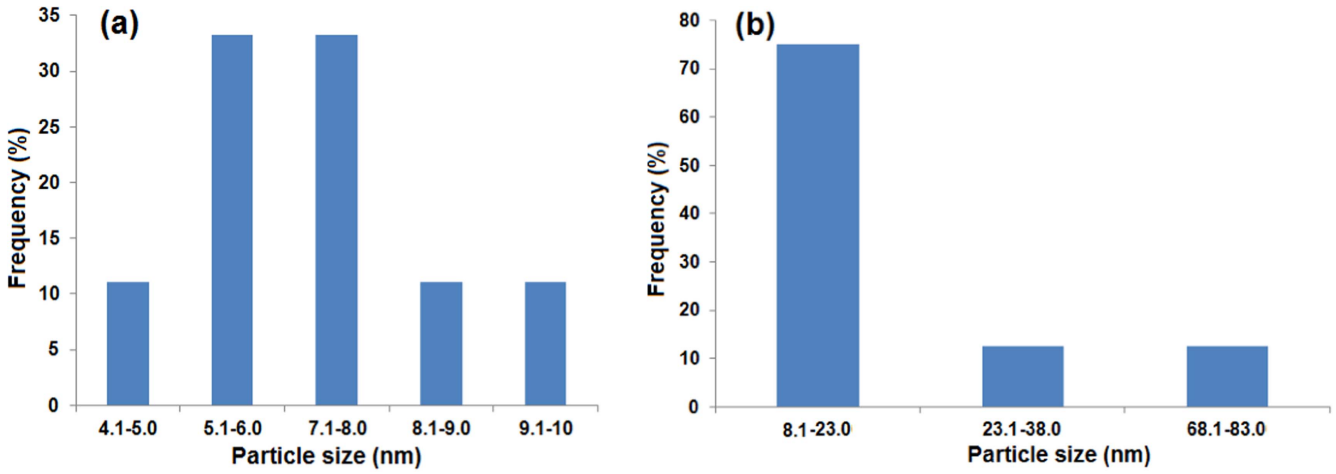

Figure 4. Particle size distribution histogram of (a) Ag/Co NPs and (b) Ag/Ni NPs capped by TOPO/OA.

spherical morphology. The diameter of particles ($n = 25$) averaged 7.02 ± 1.64 nm, with the lattice quite well-resolved and equally spaced showing their crystalline nature. The lattice spacing was calculated to be 2.30 ± 0.02 Å which is close to bulk Ag which has a lattice space of 2.27 Å. Assuming Vegard's law [47], the observed lattice spacing would yield a nominal composition of 1:2 Ag/Co for a starting composition of 1:1 Ag/Co [48]. This value should be

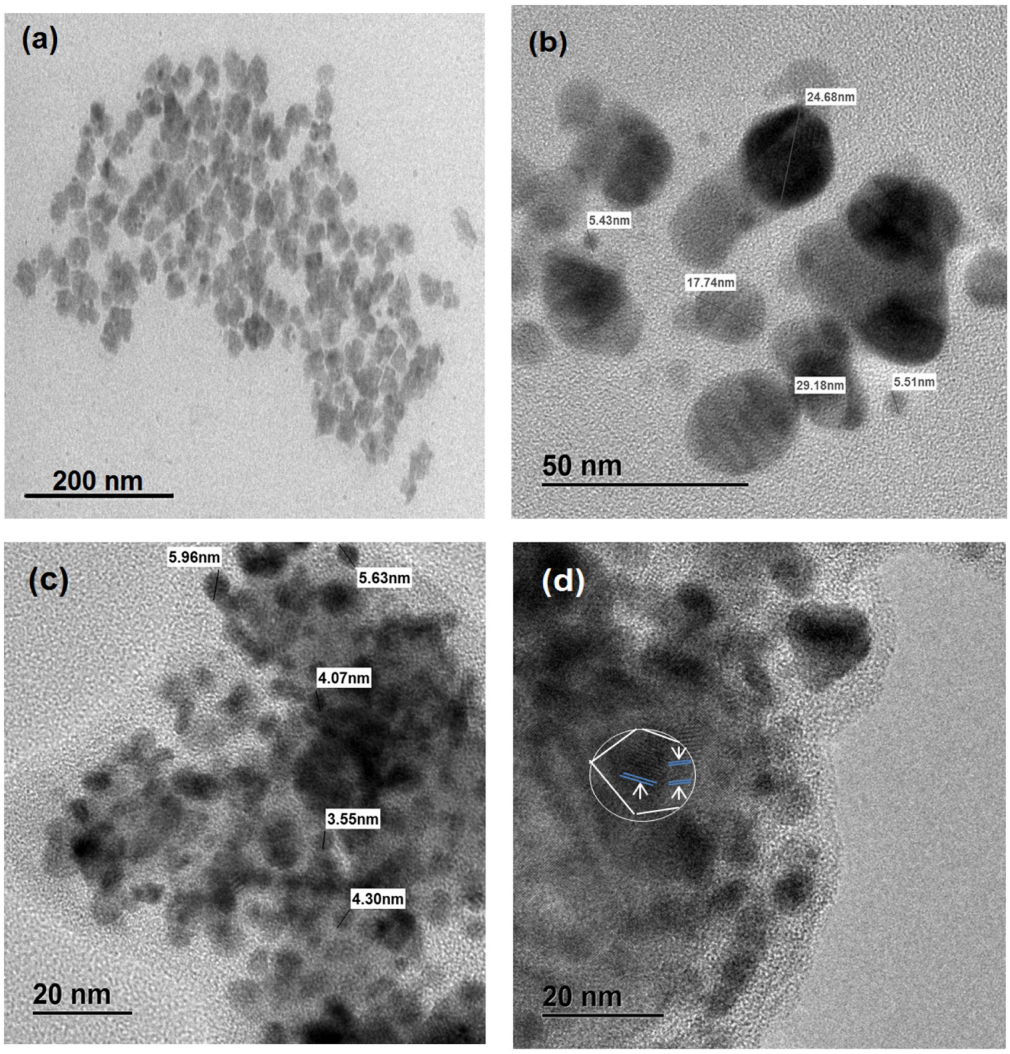

Figure 5. (a) TEM image of Ag/Pd NPs; HRTEM images of (b) Ag/Pd NPs and (c), (d) Ag/Pt NPs capped by TOPO/OA at 180 °C, 2 h.

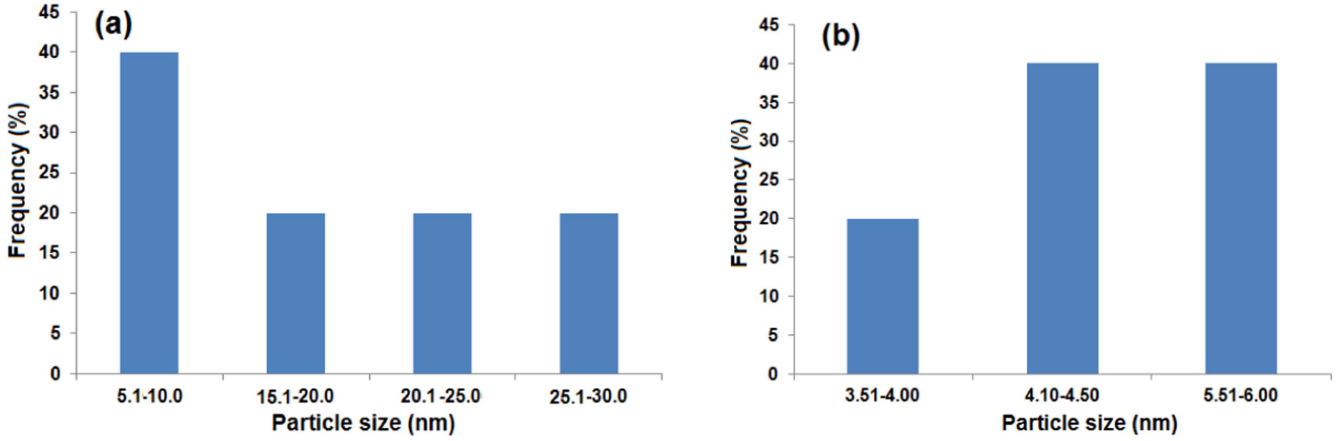

Figure 6. Particle size distribution histograms of (a) Ag/Pd NPs and (b) Ag/Pt NPs capped by TOPO/OA.

treated with some caution since a little variation in the measurement of the lattice spacing could lead to a large error in the final composition. The corresponding HRTEM image of the TOPO/OA capped Ag/Co (figure 3(c)) also shows lattice fringes. The external shell of Co surrounding the Ag core is evident in the HRTEM image (inset (e) of figure 3(c)) shown by arrows confirming the core–shell structure of the material.

The TEM image of the TOPO/OA capped Ag/Ni nanobimetallic particles (figure 3(d)) reveals their polydispersed nature corroborated by the particle size distribution

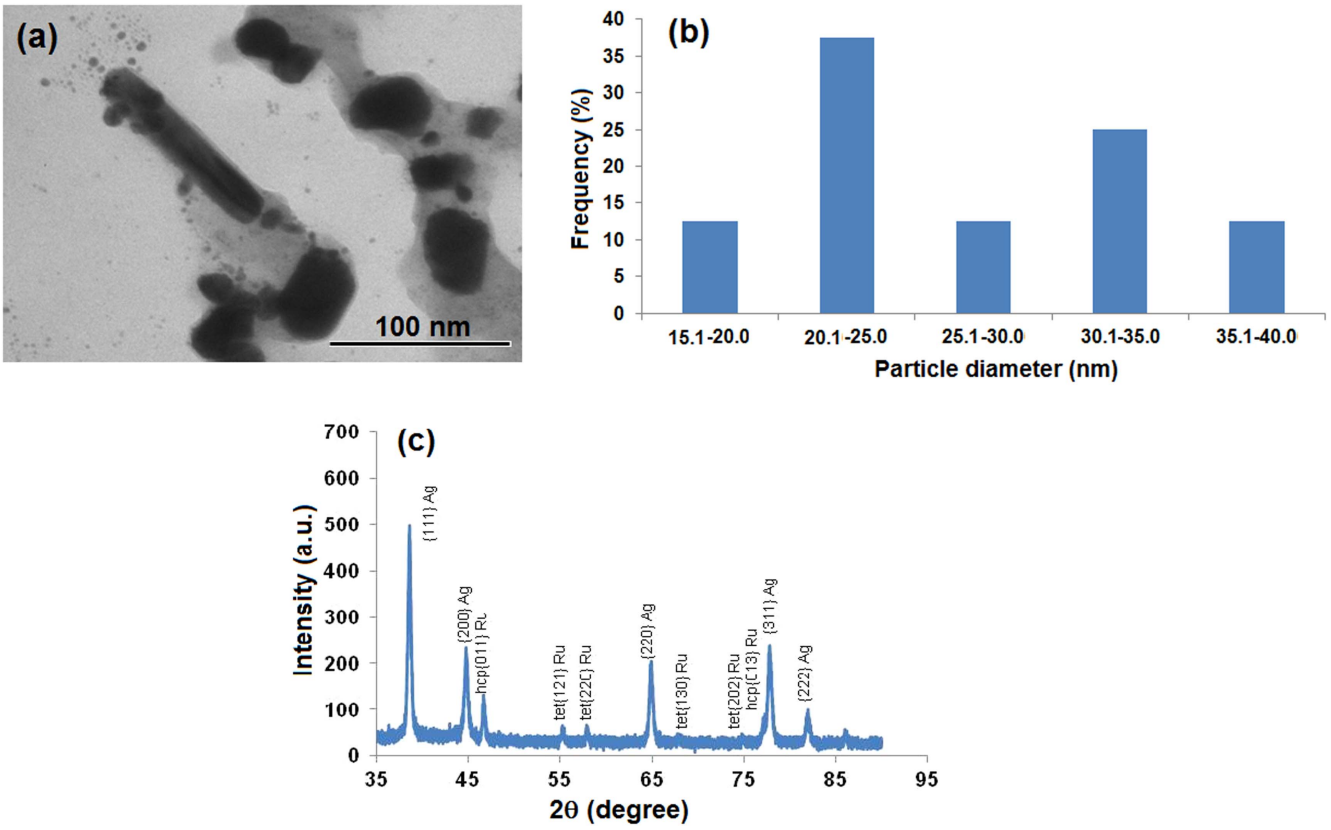

Figure 7. (a) TEM image, (b) particle diameter distribution histogram and (c) *p*-XRD pattern of Ag/Ru NPs capped by TOPO/OA at 180 °C, 2 h.

histogram (figure 4(b)); two different particle sizes were identified. Moreover, the particles showed evidence of cluster in cluster formation (figure 3(d)), in which two Ag cores were in a Ni shell. The diameter of the nanocomposites ($n = 25$) averaged 22.21 ± 10.27 nm which was also in agreement with Vegard's law [49].

The TEM images of the TOPO/OA capped Ag/Pd nanoparticles (figure 5(a)) showed monodispersed roughened edge cubic structures with the particle diameter ($n = 25$) averaged 16.50 ± 9.72 nm, which is evident by the particle size distribution histogram (figure 6(a)).

The HRTEM image (figure 5(b)) shows alloy formation with an affinity for anisotropic longitudinal growth [50]. For the formation of alloy, it was necessary that the reduction of both metal ions took place simultaneously. Therefore, different concentrations of metal ions were taken for making the mixed particles. However, the mechanism for alloying of small particles is still not clear. Kinetic consideration indicates that, for the two metals to mix, the diffusion coefficients are expected to be many orders of magnitude larger than those of the bulk materials [51].

The diameters of the TOPO/OA capped Ag/Pt ($n = 25$) and Ag/Ru nanoclusters ($n = 10$) averaged 4.70 ± 0.93 and 26.82 ± 6.35 nm respectively. The former consists of monodispersed nanosized particles with well-defined lattice spacing (figures 5(c) and (d)), this deduction is supported by the particle size distribution graph (figure 6(b)). Whereas, the latter is made up of 1D quantized polydispersed nanorods and 2D pseudo nanocubes (figure 7(a)), similar to face-centered cubic (fcc) Ag. The corresponding size distribution histogram is shown in figure 7(b). However, the mechanism of the growth process for this nanohybrid can be regarded as reaction limited, in which, etching by oxygen and Cl^- anions present in $RuCl_3$ promoted the formation of Ag/Ru nanocubes and nanorods [52]. In all, we were able to achieve stable monodispersed silver alloyed NPs with tunable morphology properties as a result of controlled capping by two organic ligands (TOPO/OA), different from our previous work when HDA was used to synthesise silver nanoalloyed particles [14].

The *p*-XRD pattern for TOPO/OA capped Ag/Ru bimetallic nanoparticles is shown in figure 7(c). We carried out *p*-XRD measurement for Ag/Ru nanoparticles due to its rareness in the literature. The appearance of well resolved reflection peaks in the *p*-XRD pattern supports the formation of nearly crystalline nanoparticles. However, the observed reflections for the bimetallic cluster were slightly different from that of individual monometallic components, showing the existence of alloy phases corresponding to peaks of fcc Ag, hexagonal close-packed (hcp) Ru and tetragonal (tet) RuO phases which portend the formation of alloyed Ag/Ru particles in agreement with TEM and optical measurement. The fcc {111} Ag plane occurred at 38.34° (2θ) and the {200} plane occurred at 44.91° (2θ) for a mole ratio 1:2 Ag/Ru. There is also an overlap between the hcp {013} Ru plane and the {311} Ag plane at 77.27°–77.69° (2θ) further establishing the presence of an alloy phase and formation of

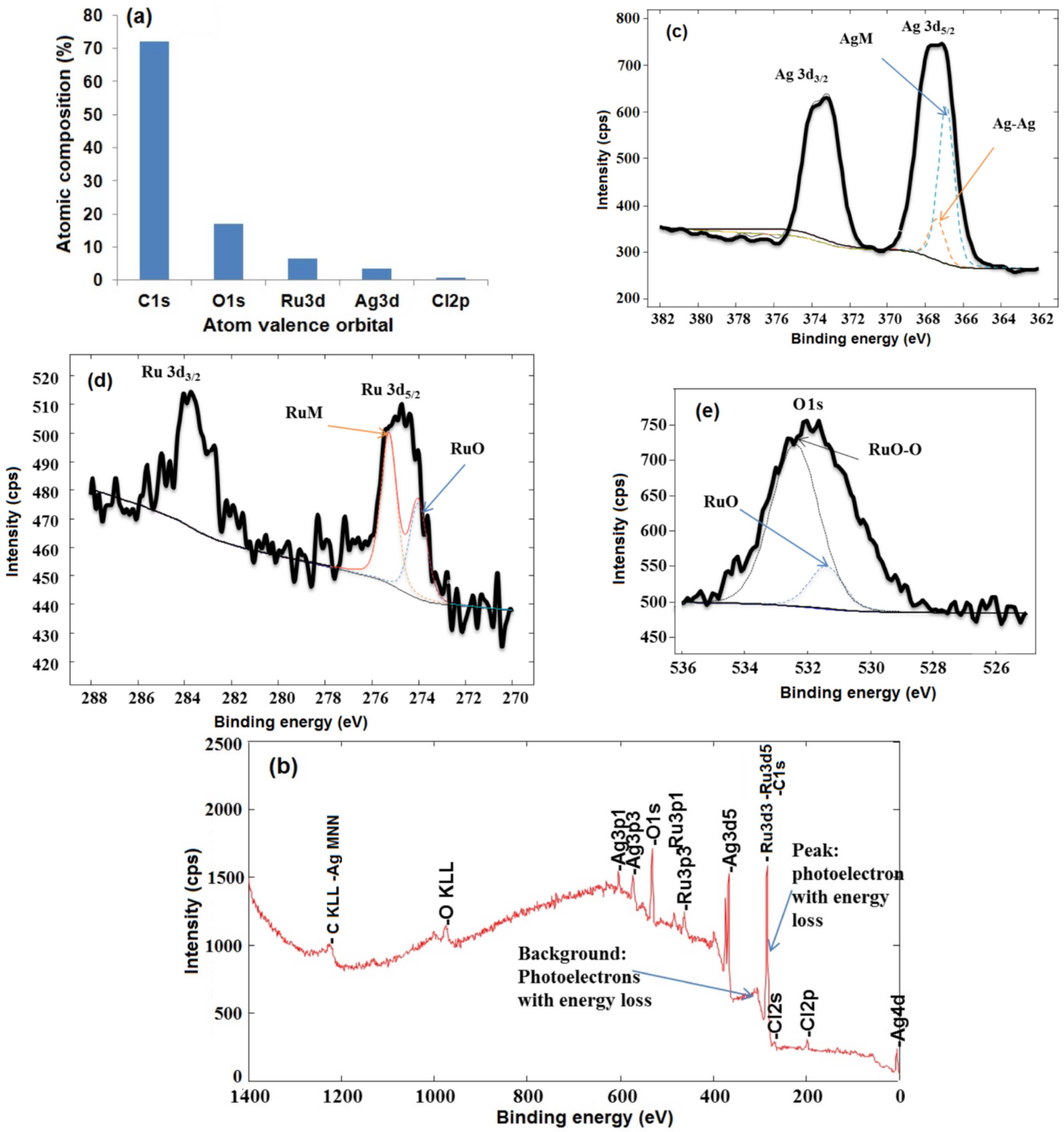

Figure 8. (a) Histogram showing % atomic composition, (b) XPS high resolution surface scan and (c) Ag (3d) core level high resolution deconvolution scan of Ag/Ru NPs capped by TOPO/OA at 180 °C, 2 h; (d) XPS high resolution scan of Ru (3d) and (e) of O(1 s) core levels.

Ag/Ru alloyed nanoparticles. The particle size calculated from the [111] peak at FWHM using the Scherrer equation was 23.07 nm, which is in good agreement with the TEM results.

3.3. XPS results

For the XPS analysis, one of the nanocomposites, Ag/Ru TOPO/OA was considered for characterization with sputtering carried out on the sample at the surface monolayers. The spectrum and the high resolution scans of the core levels of Ag/Ru nanocluster capped with TOPO/OA are presented in figure 8. The high resolution surface scan spectra of Ag/Ru NPs (figure 8(b)) showed the presence of Ag, Ru and O according to their binding energies. The stoichiometric ratio of Ag to Ru in $AgRuO_x$, determined from the wide area XPS scan was 1:1.8 (figure 8(a)).

The deconvolution of Ag ($3d_{5/2}$) core levels (figure 8(c)) resulted in a peak at 367.44 eV binding energy (BE) with an

auger parameter, $AgM_{45}N_{23}N$ of 1227.9 eV assigned to Ag, while a BE of 366.8 eV corresponding to ($3d_{5/2}$) core levels with auger parameter, O KLL of 977.4 eV was assigned to AgM. The chemical shift or change in 3d photoelectron peaks for the Ag core levels was 0.2–0.3 eV, while the 3d spin–orbit split was 6.0 eV. Both the Ag and Ru peaks were integrated as intense peaks in the spectrum. But the deconvolution of Ru ($3d_{5/2}$) core levels (figure 8(d)) resulted in a peak at 280.1 eV (BE) which was assigned to RuO [53].

The interaction between Ru and Ag made the Ag (3d) BE to increase by a factor of 0.04 eV, and Ru (3d) BE decreased obviously to 278.6 eV. The presence of Ag withdrew electrons from nearby Ru and thus made Ru electropositive, which was beneficial to produce more active sites where electrophilic oxygen species can be absorbed to increase capping group selectivity [54].

The deconvolution of XPS high-resolution scan for the O (1 s) core level (figure 8(e)) showed the presence of three different peaks. The main peak centered at 531.69 eV has been attributed to RuO–O in the $AgRuO_x$ structure, while the peak at 531.89 eV was associated with the O (1 s) in the Ru–O species. Therefore, in the Ag/Ru nanoparticles charge transfer from ruthenium to oxygen was reduced, thus increasing the shielding effect of the valence electrons in Ru ions which in turn decreased the BE of core electrons in Ru ion. This complex modification of ruthenium binding state was associated with the variation in the number of broken bonds per ruthenium ion due to quantum size effect, which led to the formation of oxygen vacancies in the host [55].

Whereas, AgRu nanoparticles in TOPO/OA matrices indicated significant reduction potential, the energy band gap of AgPt from table 1 points to the fact that it could be a likely better reducing agent for electrocatalytic reaction. This deduction indicating potential application of AgPt nanoparticles as nanocatalysts can be corroborated by its relative nanoscale dimension 4.70 ± 0.93 nm obtained from TEM images. In that order, we consider AgCo nanoparticles in TOPO/OA matrices as having a relatively small reduction potential, with an energy band gap of 2.77 eV and an average particle size of 7.02 ± 1.64 nm.

4. Conclusion

The synthesis of alloyed Ag/M nanobimetallic particles by co-precipitation route using multiple ligands, TOPO/OA to cap inorganic precursors was successfully accomplished. Characterization of the nanocomposites using optical spectroscopy showed the existence of SPB at 447 and 462 nm for TOPO/OA capped Ag/Co and Ag/Ni respectively. The electron micrograph clearly showed the evidence of a core–shell nanostructured Ag/Co NPs and a segregated alloy structure of TOPO/OA capped Ag/Pd NPs which is corroborated by the absorption spectral measurement. The *p*-XRD showed the existence of fcc with nearly pure crystalline phase, and the x-ray photoelectron spectroscopy showed the existence of Ag/M nanoalloys which were monodispersed and uniformly distributed in non-aqueous solution. The deconvolution of XPS high resolution and detailed surface elucidation of the bimetallic nanoparticles in ligand matrix revealed that their surfaces consisted of both metals which resulted into alloy or core–shell formation (figure 3(b)). Their binding energies were established showing that Ag–Ru and Ru–O bonds were formed at the corresponding BE intervals. The fcc {311} Ag plane occurred at 77.27° (2θ) and the {013} Ru plane at 77.69° (2θ) for a mole ratio 1:2 Ag/Ru. This without doubt established an overlap in the Ag/Ru planes confirming the formation of bimetallic nanoalloy.

Acknowledgments

The authors thank the National Research Foundation (NRF), South Africa through the South African Research Chair Initiative (SARChI) program for financial support. The authors also thank Professor Hendrik Swart of the University of Free-state, Bloemfontein, South Africa for XPS measurements.

References

[1] Biju V, Itoh T, Anas A, Sujith A and Ishikawa M 2008 *Anal. Bioanal. Chem.* **391** 2469
[2] Suo Y G, Zhuang L and Lu J T 2007 *Angew. Chem., Int. Ed. Engl.* **46** 2862
[3] Zhang J, Sasaki K, Sutter E and Adzic R R 2007 *Science* **315** 220
[4] Devarajan S, Bera P and Sampath S 2005 *J. Colloid Interface Sci.* **290** 117
[5] Mizukoshi Y, Fujimoto T, Nagata Y, Oshima R and Maeda Y 2000 *J. Phys. Chem.* B **104** 6028
[6] Harpeness R and Gedanken A 2004 *Langmuir* **20** 3431
[7] Henglein A 2000 *J. Phys. Chem.* B **104** 6683
[8] Hu J W, Li J F, Ren B, Wu D Y, Sun S G and Tian Z Q 2007 *J. Phys. Chem.* C **111** 1105
[9] Lee A F, Baddeley C J, Hardacre C, Ormerod R M, Lambert R M, Schmid G and West H 1995 *J. Phys. Chem.* **99** 6096
[10] Toshima N, Harada M, Yamazaki Y and Asakura K 1992 *J. Phys. Chem.* **96** 9927
[11] Flynn N T and Gewirth A A 2002 *J. Raman Spectrosc.* **33** 243
[12] Schmid G, Lehnert A, Malm J-O and Bovin J-O 1991 *Angew. Chem., Int. Ed. Engl.* **30** 874
[13] Takenaka T and Eda K 1985 *J. Colloid Interface Sci.* **105** 342
[14] Adekoya J A, Dare E O, Mesubi M A and Revaprasadu N 2015 *Physica* E **71** 70
[15] Adekoya J A, Dare E O and Mesubi M A 2014 *Adv. Nat. Sci.: Nanosci. Nanotechnol.* **5** 035007
[16] Adekoya J A, Dare E O, Mesubi M A and Revaprasadu N 2014 *J. Mater.* **2014** 184216
[17] Liz-Marzan L M and Philipse A P 1995 *J. Phys. Chem.* **99** 15120
[18] Ksar F, Ramos L, Keita B, Nadjo L, Beaunier P and Remita H 2009 *Chem. Mater.* **21** 3677
[19] Mejía-Rosales S J, Fernández-Navarro C, Pérez-Tijerina E, Blom D A, Allard L F and José-Yacaman M 2007 *J. Phys. Chem.* C **111** 1256
[20] Suo Y and Hsing I-M 2011 *Electrochim. Acta* **56** 2174
[21] Niesz K, Grass M and Somorjai G A 2005 *Nano Lett.* **5** 2238
[22] Ackerson C J, Jadzinsky P D and Kornberg R D 2005 *J. Am. Chem. Soc.* **127** 6550

[23] Büttner M, Belser T and Oelhafen P 2005 *J. Phys. Chem.* B **109** 5464
[24] Lu Y, Mei Y, Drechsler M and Ballauff M 2006 *Angew. Chem., Int. Ed. Engl.* **45** 813
[25] Shon Y-S and Cutler E 2004 *Langmuir* **20** 6626
[26] Temleton A C, Wuelfing W P and Murray R W 2000 *Acc. Chem. Res.* **33** 27
[27] Ohde H, Hunt F and Wai C M 2001 *Chem. Mater.* **13** 4130
[28] Adekoya J A, Dare E O, Mesubi M A and Revaprasadu N 2015 *J. Phys. Chem. Solids* **86** 155
[29] Sergeev G B 2001 *Russ. Chem. Rev.* **70** 809
[30] Lee Y W, Kim M, Kim Z H and Han S W 2009 *J. Am. Chem. Soc.* **131** 17036
[31] Adekoya J A, Dare E O, Mesubi M A, Nejo A A, Swart H C and Revaprasadu N 2014 *Res. Phys.* **4** 12
[32] Slezov V V, Schmelzer J W P and Abyzov A S 2005 *A New Method of Determination of the Coefficients of Emission in Nucleation Theory* ed J W P Schmelzer (Weinheim: Wiley-VCH Verlag GmbH & Co) p 39
[33] Soni P L and Soni V 2013 *Coordination Chemistry: Metal Complexes* (California: CRC Press)
[34] Hoffman M, Martin S, Choi W and Bahnemann D 1995 *Chem. Rev.* **95** 69
[35] Lu L, Eychmüller A, Kobayashi A, Hirano Y, Yoshida K, Kikkawa Y, Tawa K and Ozaki Y 2006 *Langmuir* **22** 2605
[36] Koichi A, Makoto F, Carsten R, Junji T, Hirotaka M, Yoshimichi O, Naoya Y and Toshiya W 2008 *Am. Chem. Soc.* **130** 1676
[37] Gulino A, Dapporto P, Rossi P and Fragala I 2003 *Chem. Mater.* **15** 3748
[38] Kumar R V, Diamant Y and Gedanken A 2000 *Chem. Mater.* **12** 2301
[39] Michael D I, Buchholz D B, Alexander W H, Robert P H C and Tobin J M 2008 *p*-type semiconducting nickel oxide as an efficiency-enhancing anode interfacial layer in polymer bulk-eterojunction solar cells *Proc. Natl Acad. Sci.* **105** 2783
[40] Sarkar B, Chakrabarti K, Das K and De S K 2012 *J. Phys. D: Appl. Phys.* **45** 505304
[41] Fischer R, Schuppler S, Fischer N, Fauster T and Steinmann W 1993 *Phys. Rev. Lett.* **70** 654
[42] Kohler A, Wilson J S, Friend R H, Al-Suti M K, Khan M S, Gerhard A and Bassler H *J. Chem. Phys.* **116** 9457
[43] Wilson J S, Kohler A, Friend R H, Al-Suti M K, Al-Mandhary M R A, Khan M S and Raithby P R 2000 *J. Chem. Phys.* **113** 7627
[44] Gao J, Fu J, Lin C, Lin J, Han Y, Yu X and Pan C 2004 *Langmuir* **20** 9775
[45] Safin D A, Mdluli P S, Revaprasadu N, Ahmad K, Afzaal M, Helliwell M, O'Brien P, Shakirova E R, Babashkina M G and Klein A 2009 *Chem. Mater.* **21** 4233
[46] Kulmala S and Suomi J 2003 *Anal. Chim. Acta* **500** 21
[47] Leppert L, Albuquerque R Q and Kummel S 2012 *Phys. Rev.* B **86** 241403
[48] Xiong L and Manthiram A 2005 *J. Electrochem. Soc.* **152** 697
[49] Leppert L, Albuquerque R Q, Foster A S and Kummel S 2013 *J. Phys. Chem.* C **117** 17268
[50] Chaoying N, Puthussericka A H and Eric W K 2005 *Langmuir* **21** 3334
[51] Yasuda H and Mori H 1992 *Phys. Rev. Lett.* **69** 3747
[52] Siekkinen A R, McLellan J M, Chen J and Xia Y 2006 *Chem. Phys. Lett.* **432** 491
[53] Moulder J F, Stickle W F, Sobol P E and Bomben K D 1995 *Standard XPS Spectra of Elements* ed J Chastain and R C King Jr (Minnesota: Physical Electronics Inc.) p 30
[54] Jun Y, Jim Y L and Heng P T 2006 *Plasmonics* **1** 67
[55] Harrak A E, Carrot G, Oberdisse J, Eychenne-Baron C and Boue F 2004 *Macromolecules* **37** 6376